Supplementary information

Band Splitting and enhanced Charge Density Wave Modulation in

Mn-implanted CsV$_3$Sb$_5$

Xiaoxu Lei, ‡[a,b] Pengdong Wang,‡ [b], Mengjuan Mi,[c] Yan Zhang,[d] Aixi Chen,[b] Liwu Cai,[b,e] Ting Wang, [a,b] Rong Huang,[b] Yilin Wang,[*c] Yiyao Chen[*b] and Fang-Sen Li[*a, b]

[a] School of Nano-Tech and Nano-Bionics, University of Science and Technology of China, Hefei 230026, China

[b] Vacuum Interconnected Nanotech Workstation Suzhou Institute of Nano-Tech and Nano-Bionics, Chinese Academy of Sciences, Suzhou 215123, China

[c] School of Microelectronics Shandong Technology Center of Nanodevices and Integration State Key Laboratory of Crystal Materials, Shandong University. Jinan 250100, China.

[d] CAS Key Laboratory of Nanophotonic Materials and Devices & Key Laboratory of Nanodevices and Applications, i-Lab, Suzhou Institute of Nano-Tech and Nano-Bionics, Chinese Academy of Sciences, Suzhou 215123, China

[e] Nano Science and Technology Institute, University of Science and Technology of China, Suzhou 215123, China
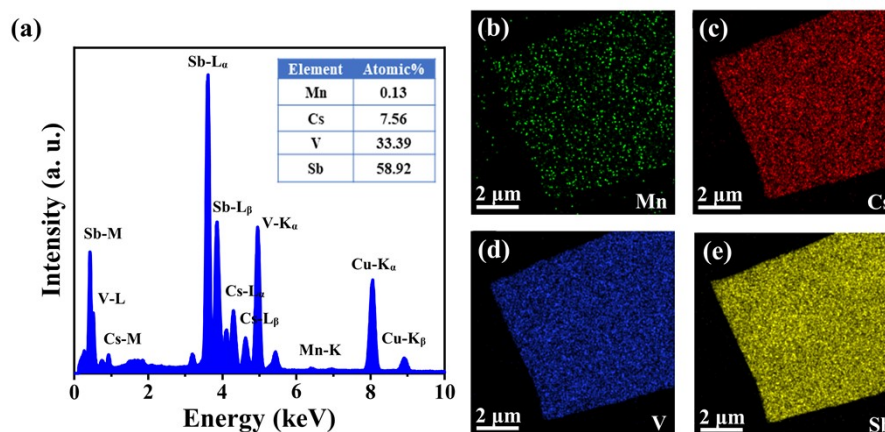
Additional characterizations results

Fig. S1 The chemical composition of Mn-doped CVS samples. (a) The EDX spectrum of Mn-doped CVS. (b) - (e) The corresponding EDX elemental mappings of Mn, Cs, V and Sd, respectively, suggesting uniformed Mn doping in CVS. The elemental ratio of CVS measured in the experiment is different from 1:3:5, which may be due to the mass loss of Cs during sample preparation and FIB process.
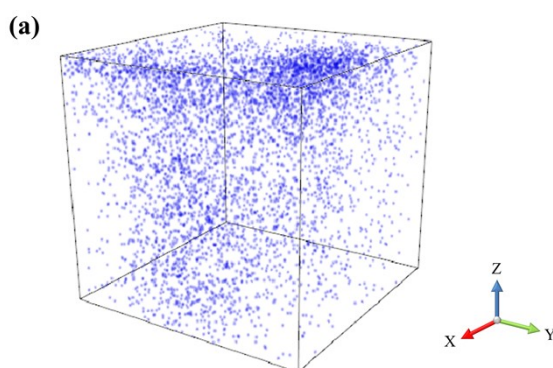

Fig. S2 The 3D depth profiling of uncleaved Mn-doped CVS by using TOF-SIMS, and the dissection depth can reach 1480 nm, showing rather uniform distribution and deep implantation up to micron thickness.
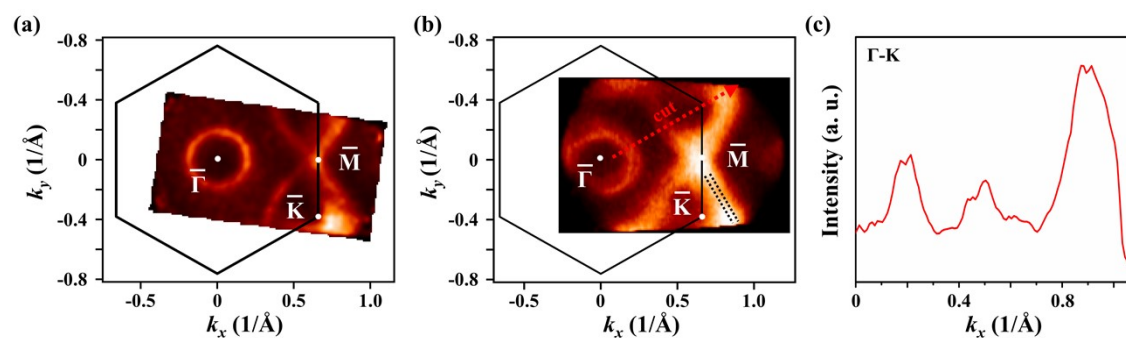

Fig. S3 Fermi surface (FS) of (a) pristine CVS and (b) Mn-doped CVS. (c) The momentum distribution curve (MDC) in Mn-doped CVS, which cutting along the red dashed line (Γ-K direction) in (b). The two peaks of band splitting are marked by the black dashed lines in (b).
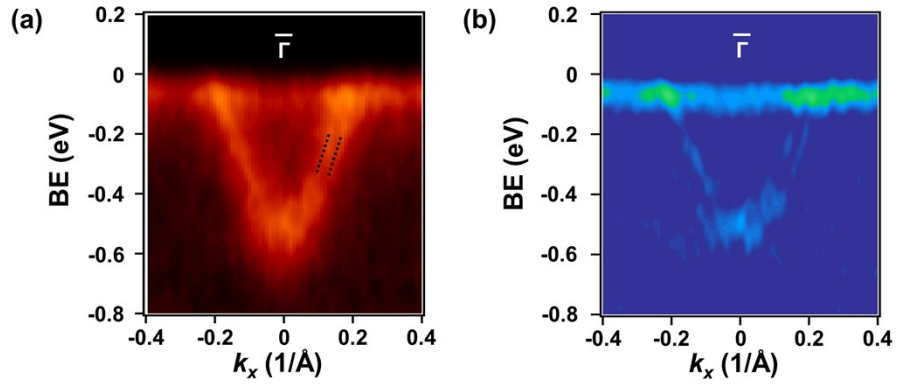
Fig. S4 The ARPES spectra measured at temperature of 300 K along the Γ-K direction in (a) Mn-doped samples. (b) Corresponding second derivative of the energy distribution curves (EDC), indicating the energy band splitting phenomenon still occurred at room temperature.
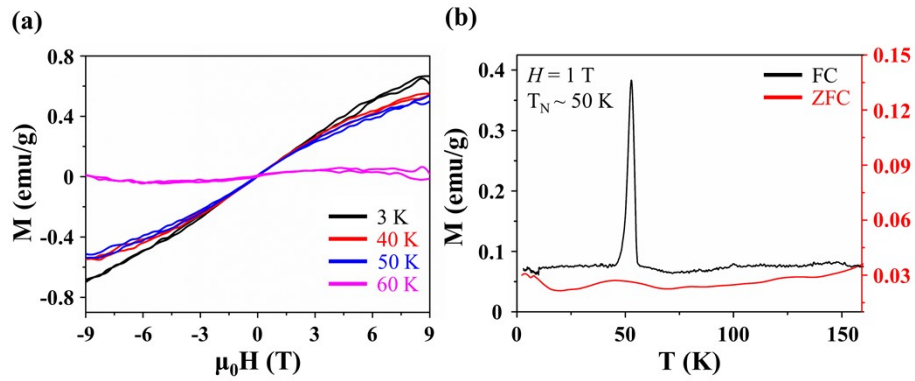

Fig. S5 Magnetic properties of Mn-doped CVS samples. (a) Isothermal magnetization of Mn-doped CVS samples under a magnetic field H//ab at different temperatures. Each temperature provides hysteresis loops from -9 T to 9 T. (b) Temperature dependence of magnetization (M–T, a) in zero-field cooled (ZFC, red) mode and field cooled (FC, black) of Mn-doped sample under magnetic fields H // c*, showing a clear peak similar to the weak interlayer antiferromagnetic coupling.
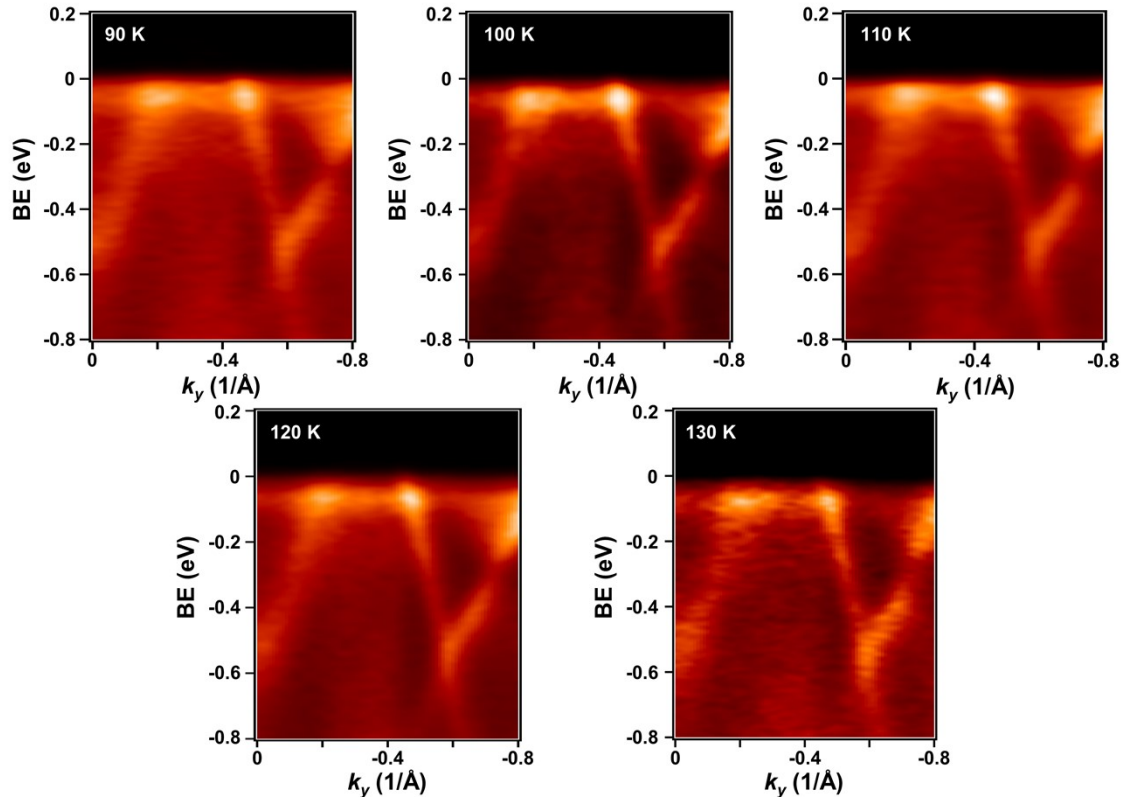
Fig. S6 The energy band dispersion along the Γ-K direction from 90 K to 130 K at 10 K interval, showing the temperature evolution of the Dirac cone gap in Mn-doped CVS.
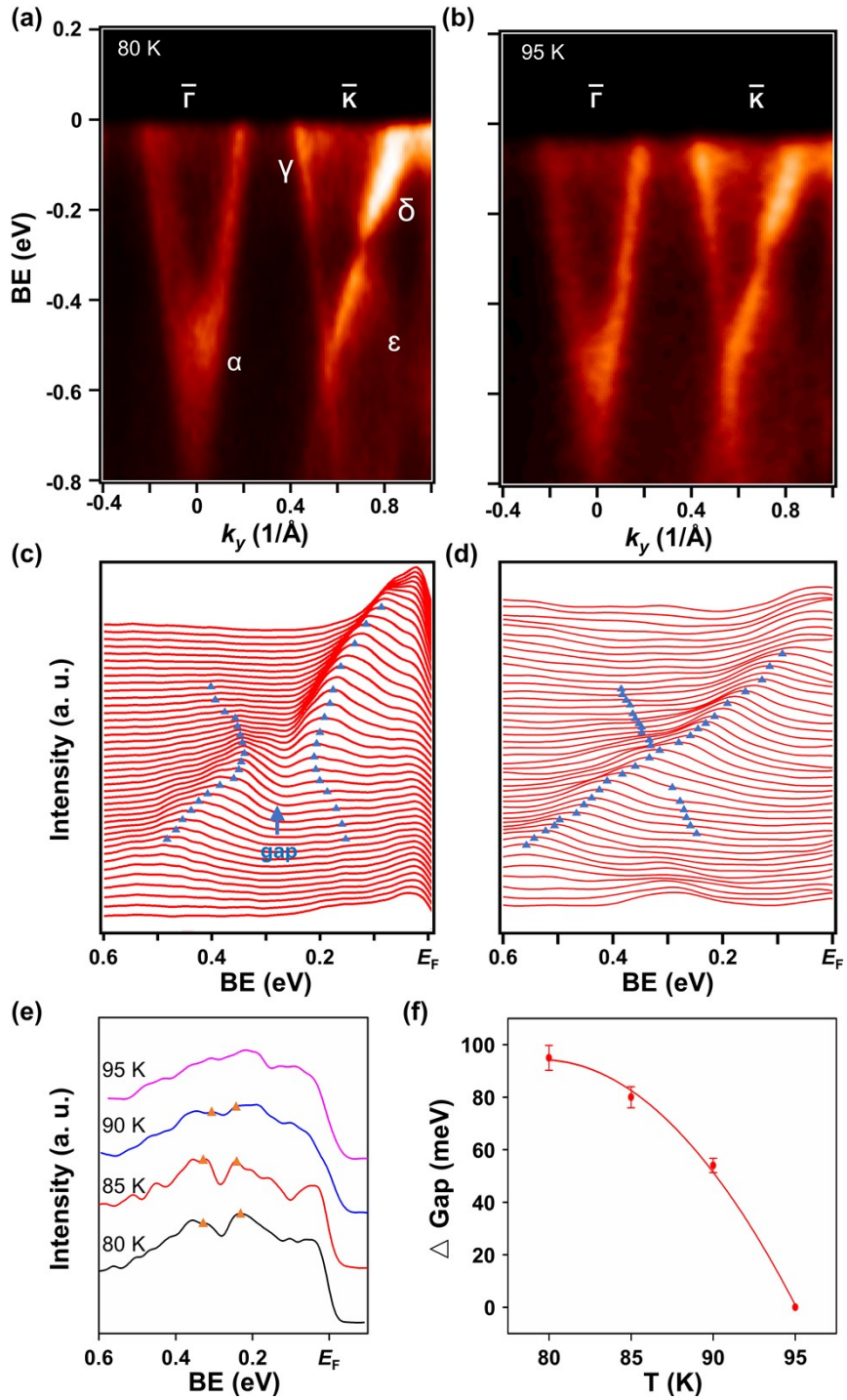
Fig. S7 The Dirac cone gap at K point of Pristine CVS. (a) and (b) Energy band dispersion measured at T = 80 K and 95 K. Corresponding EDC in (c) and (d), respectively. (e) Temperature evolution of the Dirac cone gap are performed from 80 K to 95 K at 5 K interval, and (f) the CDW gap size fitted curves, showing the Dirac cone gap becomes smaller with increasing temperature and disappears at 95 K, same as the CDW transition temperature of 94 K.
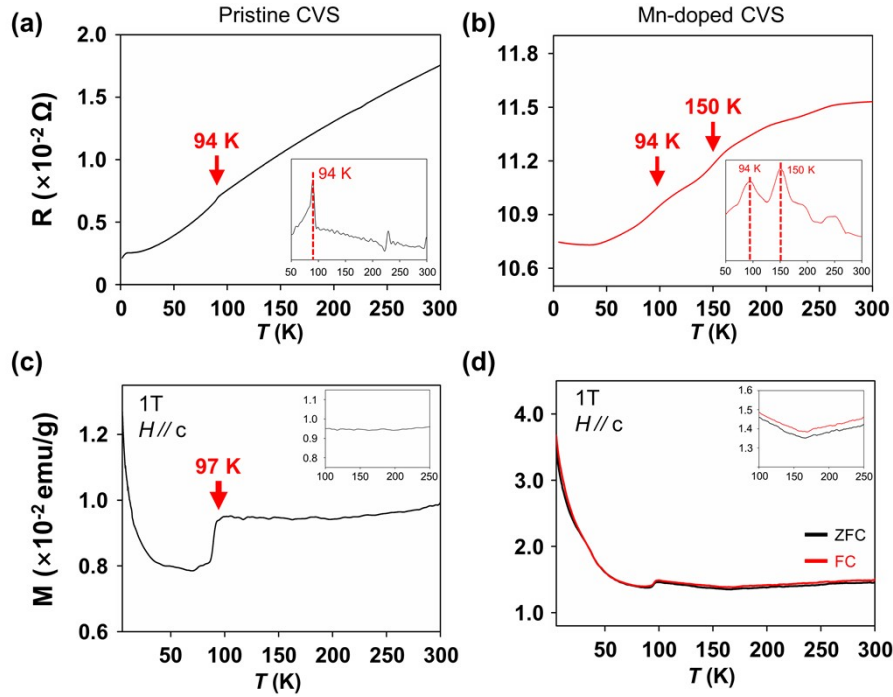
Fig. S8 Transport and magnetic susceptibility measurements of Pristine and Mn-doped CVS. (a), (b) The temperature dependence of single crystal and Mn-doped CVS resistance, respectively. The inset in (a) shows the derivative of (a), indicating the presence of an anomaly T_{CDW} at 94 K. The T_{CDW} for Mn-doped CVS is approximately 94 K and 150 K in (b), suggesting the CDW transition in Mn-doped CVS is significantly enhanced. (c), (d) The magnetic susceptibility under 1 T for ZFC (Black) and FC (Red) measurement along the *c* direction. The inset shows the zoom-in data among 100 K~250 K.
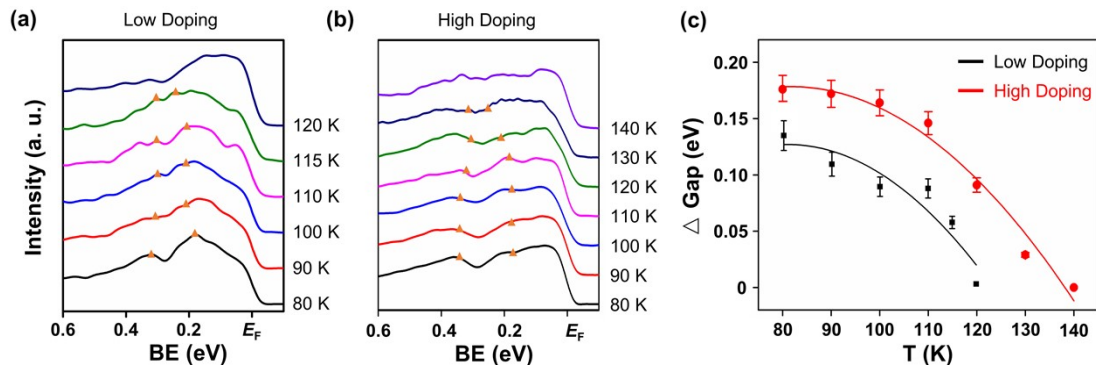

Fig. S9 (a), (b) Temperature evolution of the Dirac cone gap in CVS under different Mn doping concentrations. (c) The Dirac cone gap size was extracted and fitted. The black and red curves represent low doping and high doping CVS. The Dirac cone gap decreased with temperature. The Dirac cone gap of low-doping samples nearly disappears at 120 K ± 5 K and the high doping disappears at 135 K ± 5 K respectively.
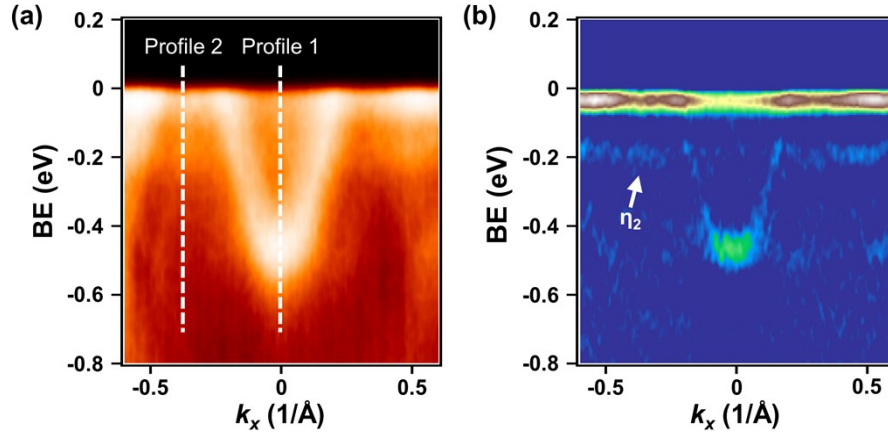
Fig. S10 (a) The ARPES intensity map and (b) corresponding second derivative near the Γ point in Mn-doped samples measured at 80 K. Though the long-time signal accumulation, the second Kondo resonance peak η_2 at -0.2 eV was clear. The profiles1 and 2 represent the extracted positions of EDC in Figure 4.
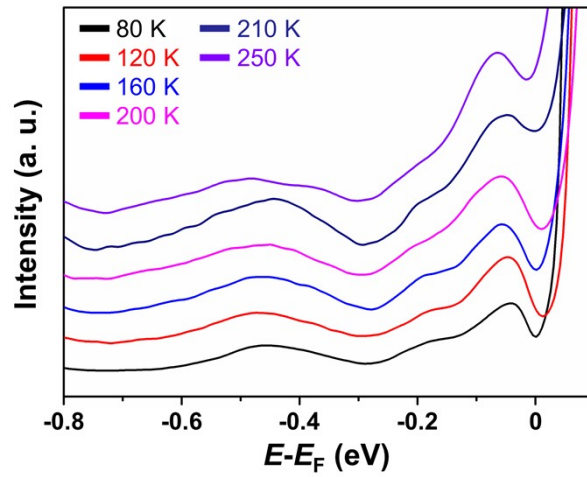

Fig. S11 Temperature evolution of the EDC around Γ point after deducting the backbone. Due to the strong density of states near the Fermi level, the first Kondo resonance peak could not be observed.